JOURNAL OF MATERIALS SCIENCE 30 (1995) 5056–5064

Experimental and theoretical phase diagrams of the iron-rich Fe–Si–Ge ordering system

T. KOZAKAI, T. MIYAZAKI
Nagoya Institute of Technology, Nagoya 466, Japan

The phase separation in iron-rich Fe–Si–Ge ternary alloys was investigated by means of transmission electron microscopy. The phase separations into A2 and $D0_3$ were recognized in several alloys in addition to the phase separation into B2 and $D0_3$ which has already been found in Fe–Si and Fe–Ge binary systems. On the basis of TEM observations, isothermal section diagrams are proposed for the iron-rich corner at 823, 873, 923 and 973 K. The A2 + $D0_3$ two-phase field exists in a band-shaped region at 823 K. With increase in temperature, the A2 + $D0_3$ field gradually shrinks and is eventually replaced at 973 K with the B2 + $D0_3$ field, which extends from both the Fe–Si and Fe–Ge binary sides. The phase diagrams were well reproduced by the calculations based on the so-called Bragg–Williams–Gorsky approximation, taking account of the chemical and magnetic pair interactions up to the second nearest neighbour. The effects of the magnetism on the equilibria are discussed.

1. Introduction

It is well known that Fe–Si binary alloy, a typical ordering alloy system, has a two-phase field consisting of B2 and $D0_3$ ordered phases. Hence, a number of researches have experimentally [1–3] and theoretically [4] been performed on the phase separation and phase diagram of this system. Such a phase separation into B2 and $D0_3$ ordered phases has recently also been found in an Fe–Ge binary system by Nishizawa's group [5]. We have partially investigated the process of phase separation in Fe–Si–Ge ternary alloys and found the phase separation in disordered A2 and ordered $D0_3$ phases in the band-shaped region of the iron-rich corner [6, 7]. However, details of the phase separation and the phase diagram of this alloy system have not yet been reported.

In the present work, we first investigated the microstructures experimentally obtained for the iron-rich Fe–Si–Ge ternary alloys and represented the isothermal section diagrams determined by the experimental results. Second, calculations of the phase diagrams were performed on the basis of the Bragg–Williams–Gorsky (B–W–G) model where the chemical and magnetic interactions up to the second nearest neighbour atoms were taken into account. The ferro-magnetic effect on the phase separation is discussed on the basis of the calculation results.

2. Experimental procedure

Many Fe–Si–Ge alloys prepared from 99.98 at % Fe, 99.99 at % Si and 99.99 at % Ge in a vacuum induction furnace were remelted in a quartz tube of 7 mm diameter and then quenched directly on to a steel roll rotating at a high speed. The ribbon specimen obtained was about 1 mm wide and 20–30 μm thick. The chemical compositions of the ribbons are shown in Fig. 1. The ribbons were isothermally annealed at 823, 873, 923 and 973 K for long durations in evacuated quartz tubes. The microstructures were observed using a transmission electron microscope (JEM 2000FX and 2000EX operated at 200 kV). Thin foils for TEM were prepared by electro-polishing in a solution of $HClO_4$ (9% by volume) and CH_3OH (91%). In the TEM observation, the incident electron beam was directed parallel to the [0 1 1] direction of the thin foil, resulting in a simultaneous formation of 2 0 0 and 1 1 1 superlattice spots in one reflection pattern.

Thermomagnetic analyses on the liquid-quenched specimens were performed to obtain the composition dependence of the Curie temperature.

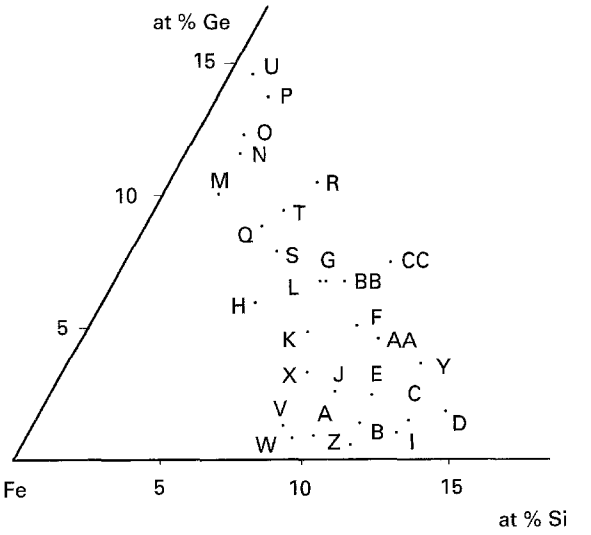

Figure 1 Chemical compositions of the Fe–Si–Ge ternary alloys used.

0022–2461

TABLE I Stable microstructures of Fe–Si–Ge alloys annealed at various temperatures. Alloys are divided into three groups. Group I, no phase separation; group II, A2 + $D0_3$ phase separation, group III, A2 + $D0_3$ and B2 + $D0_3$ phase separations

Alloy	Temperature				Group
	823 K	873 K	923 K	973 K	
A	A2	A2	A2	A2	I
M	A2	A2	A2	A2	
V	A2	–[a]	–[a]	–[a]	
W	A2	–	–	–	
AA	$D0_3$	$D0_3$	$D0_3$	–	
BB	$D0_3$	$D0_3$	$D0_3$	$D0_3$	
P	$D0_3$	$D0_3$	$D0_3$	$D0_3$	
C	$D0_3$	$D0_3$	$D0_3$	$D0_3$	
D	$D0_3$	$D0_3$	$D0_3$	$D0_3$	
Y	$D0_3$	–	–	–	
U	–	–	–	$D0_3$	
CC	$D0_3$	–	–	–	
H	A2 +$D0_3$	A2	A2	A2	II
N	A2 +$D0_3$	A2	A2	A2	
Q	A2 +$D0_3$	A2 +$D0_3$	A2	A2	
S	A2 +$D0_3$	A2 +$D0_3$	A2 +$D0_3$	A2	
X	A2 +$D0_3$	A2 +$D0_3$	B2	B2	
R	A2 +$D0_3$	$D0_3$	$D0_3$	$D0_3$	
I	A2 +$D0_3$	B2 +$D0_3$	B2 +$D0_3$	B2	III
J	A2 +$D0_3$	A2 +$D0_3$	B2 +$D0_3$	B2	
K	A2 +$D0_3$	A2 +$D0_3$	B2 +$D0_3$	B2	
L	A2 +$D0_3$	A2 +$D0_3$	A2 +$D0_3$	B2 +$D0_3$	
G	A2 +$D0_3$	A2 +$D0_3$	–	B2 +$D0_3$	
O	–	A2 +$D0_3$	–	B2 +$D0_3$	
T	A2 +$D0_3$	A2 +$D0_3$	A2 +$D0_3$	B2 +$D0_3$	
E	A2 +$D0_3$	A2 +$D0_3$	B2 +$D0_3$	$D0_3$	
F	A2 +$D0_3$	A2 +$D0_3$	B2 +$D0_3$	$D0_3$	
Z	B2 +$D0_3$	–	B2	–	
B	–	B2 +$D0_3$	–	B2	

[a] Indicates no observation, for all entries.

3. Results

3.1. Microstructures

Microstructures obtained are summarized in Table I. It is clear from the table that structural change is classified into three groups. In the group I the alloys show no phase separation. The alloys in the group II indicate a phase separation into A2 and $D0_3$ in the low-temperature range, but A2, B2 and $D0_3$ single phases at high temperature. Group III consists of the alloys which show not only the A2 + $D0_3$ phase separation but also the phase separation into B2 and $D0_3$ ordered phases. Examples of microstructures for each group will be represented below.

3.1.1. No-phase separation (group I)

The photographs in Fig. 2 are taken from Fe–13.0 at %Si–1.6 at %Ge alloy (C) annealed at 923 K for 350 ks. In both the dark-field images Fig. 2c and d, no contrast relating to phase separation is observed, except that of anti-phase boundaries. This means that this alloy is ordered as in a whole $D0_3$.

3.1.2. A2 + $D0_3$ phase separation (groups II, III)

Fig. 3 shows the microstructures and electron diffraction pattern of Fe–7.3at % Si–6.9at% Ge alloy (L) annealed at 923 K for 350 ks. Band-shaped contrasts are seen in the bright-field image (a), indicating a phase separation. Both the dark-field images from 2 0 0 (c) and 1 1 $\bar{1}$ (d) superlattice spots show the same microstructure, consisting of A2 and $D0_3$ phases, so that the alloy decomposes into $D0_3$ and A2.

Fig. 4 shows photographs of Fe–5.7 at % Si–6.1 at %Ge alloy (H) annealed at 823 K for 2600 ks. Rod- or lens-like precipitates are observed in a bright-field image (a). These precipitates are brightly illuminated in 2 0 0 (c) and 1 1 1 (d) dark-field images, being surrounded with a dark area of A2 phase.

3.1.3. B2 + $D0_3$ phase separation (group III)

When alloy L is aged at 973 K for 170 ks, the microstructure in Fig. 5 appears. There are two kinds of ordered regions having different brightness in a 2 0 0 dark-field image (a), being different from the microstructure of Fig. 3: one is a phase brightly illuminated not only in the 2 0 0 dark-field image but also in the 1 1 $\bar{1}$ image (b), and the other is a dark phase in the 1 1 $\bar{1}$ image. Thus, the alloy decomposes into B2 and $D0_3$ phases.

Fig. 6 shows the microstructures of Fe–12.6 at % Si–1.2 at % Ge alloy (I) annealed at 923 K for 350 ks. These images show a similar contrast to the photographs in Fig. 5: there are two kinds of ordered phase, B2 and $D0_3$.

3.2. Curie temperature

An example of thermo-magnetization curves is shown in Fig. 7. The magnetization of Fe–9.6 at % Si–7.6 at % Ge (CC) alloy gradually decreases and drops abruptly near the Curie temperature, 918 K. The measured Curie temperatures of the several liquid-quenched alloys are summarized in Fig. 8. The lower the iron content of the alloy, the lower is the Curie temperature. The solid straight lines, which are given theoretically, will be discussed later.

3.3. Isothermal section diagrams

Many observations of microstructures are summarized as isothermal section diagrams in Fig. 9. At 823 and 873 K, the A2 + $D0_3$ two-phase field, which has not been found in Fe–Si and Fe–Ge binary systems, appears on the boundary between A2 and $D0_3$ single-phase fields. With increase in temperature, the A2 + $D0_3$ field is reduced in area and is replaced by the B2 + $D0_3$ fields. At 973 K, the A2 + $D0_3$ field eventually disappears. The appearance of (A2 + $D0_3$) in ternary system has already been found in other iron-based ordering ternary systems, such as Fe–Al–Ge [8], Fe–Si–V [7, 9, 10] and Fe–Si–Al [11].

4. Discussion

4.1. Calculation of phase diagrams

Based upon the Bragg–Williams–Gorsky model, the isothermal section diagrams were calculated at 823,

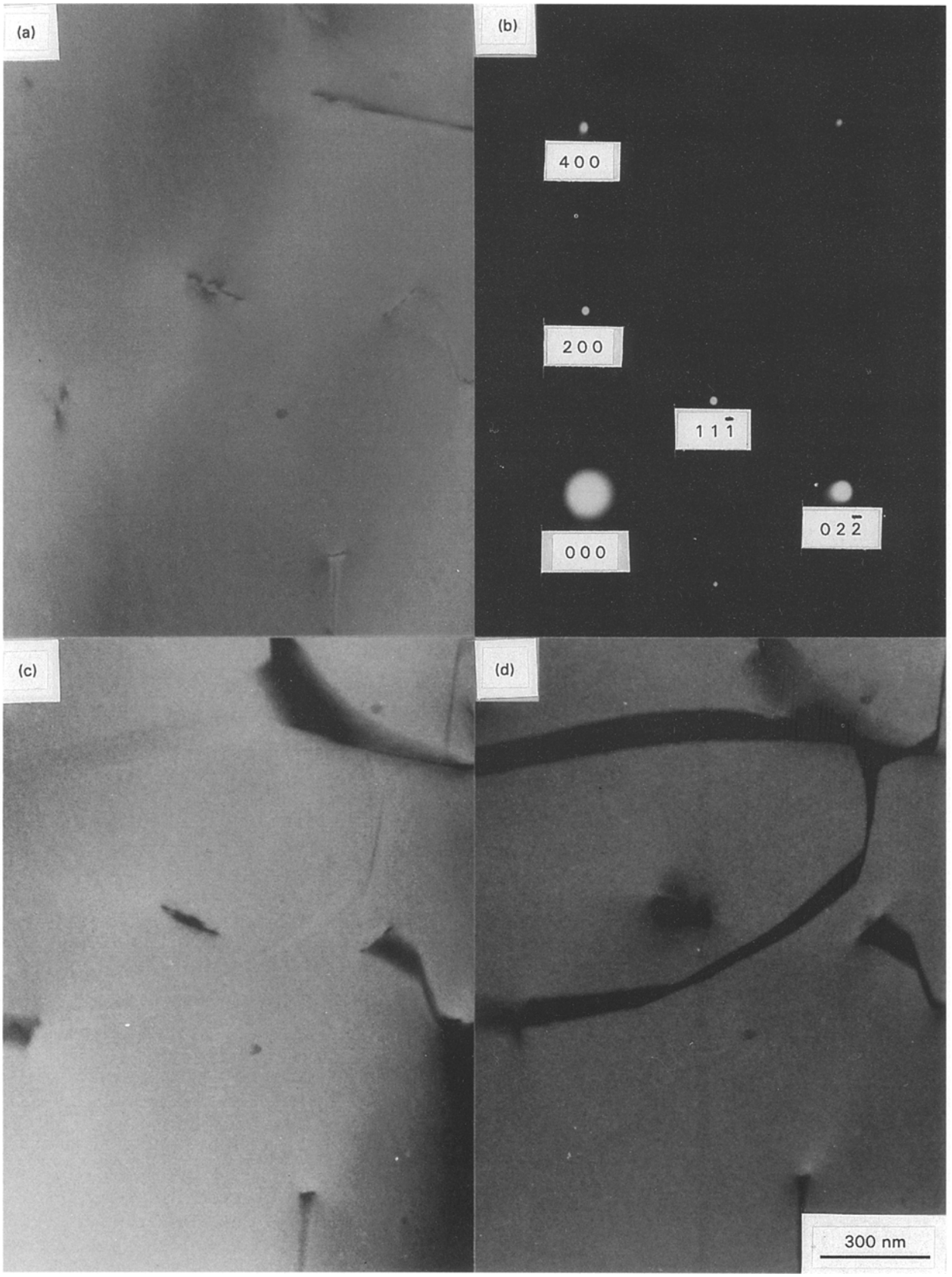

Figure 2 $D0_3$ single-phase micrographs of Fe–13.0 at % Si–1.6 at % Ge alloy (C) annealed at 923 K for 350 ks. (a) Bright-field image, (b) electron diffraction pattern of (0 1 1), (c, d) dark-field images taken from 2 0 0 and 1 1 $\bar{1}$ superlattice reflections, respectively.

873, 923 and 973 K. The theoretical basis is omitted in the present paper, because it was shown in our previous papers [12, 13].

The numerical values of the chemical interchange energies, $W^{(k)}_{FeSi}$, $W^{(k)}_{FeGe}$ and $W^{(k)}_{SiGe}$, and the magnetic interchange energy, $J^{(k)}_{FeFe}$, are listed in Table II.

First, the ferro/para magnetic transformation lines were estimated at several temperatures, as shown in Fig. 8. The straight solid lines in Fig. 8, which were calculated, are consistent with the empirical Curie temperatures. Thus, the magnetic excess free energy is reasonably evaluated in the ternary system.

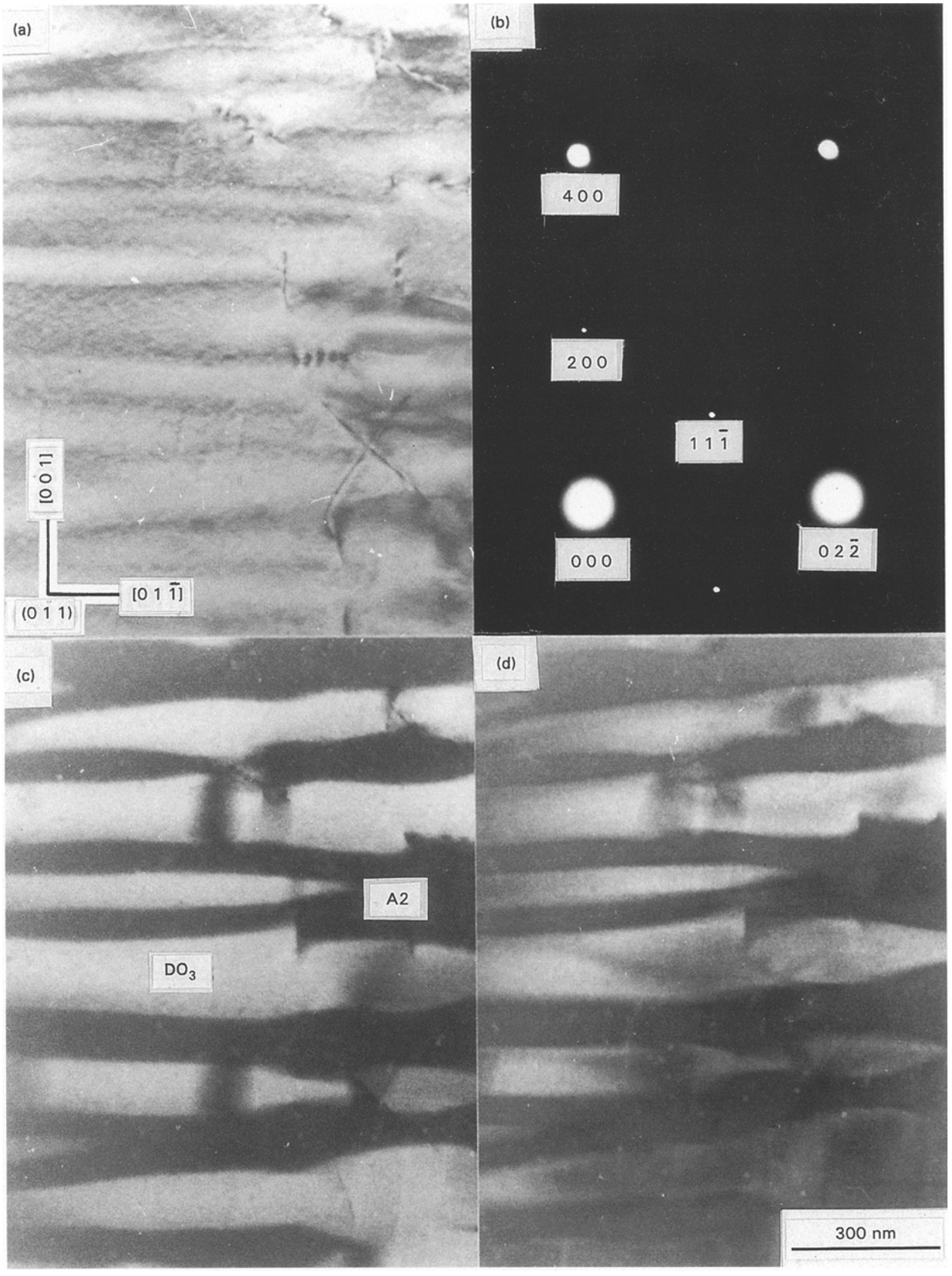

Figure 3 Transmission electron micrographs of Fe–7.3 at % Si–6.9 at % Ge alloy (L) annealed at 923 K for 350 ks. (a) Bright-field image, (b) diffraction pattern of (0 1 1), (c, d) 2 0 0 and 1 1 $\bar{1}$ dark-field images, respectively.

The isothermal section diagrams, calculated for various temperatures, are shown in Fig. 10. The characteristics of the experimental phase diagrams are well reproduced; the A2 + $D0_3$ band-shaped field existing at lower temperature, retrogrades with increase in temperature and eventually fades out at 973 K. The B2 + $D0_3$ field, instead of A2 + $D0_3$, expands from the Fe–Si and Fe–Ge binary sides.

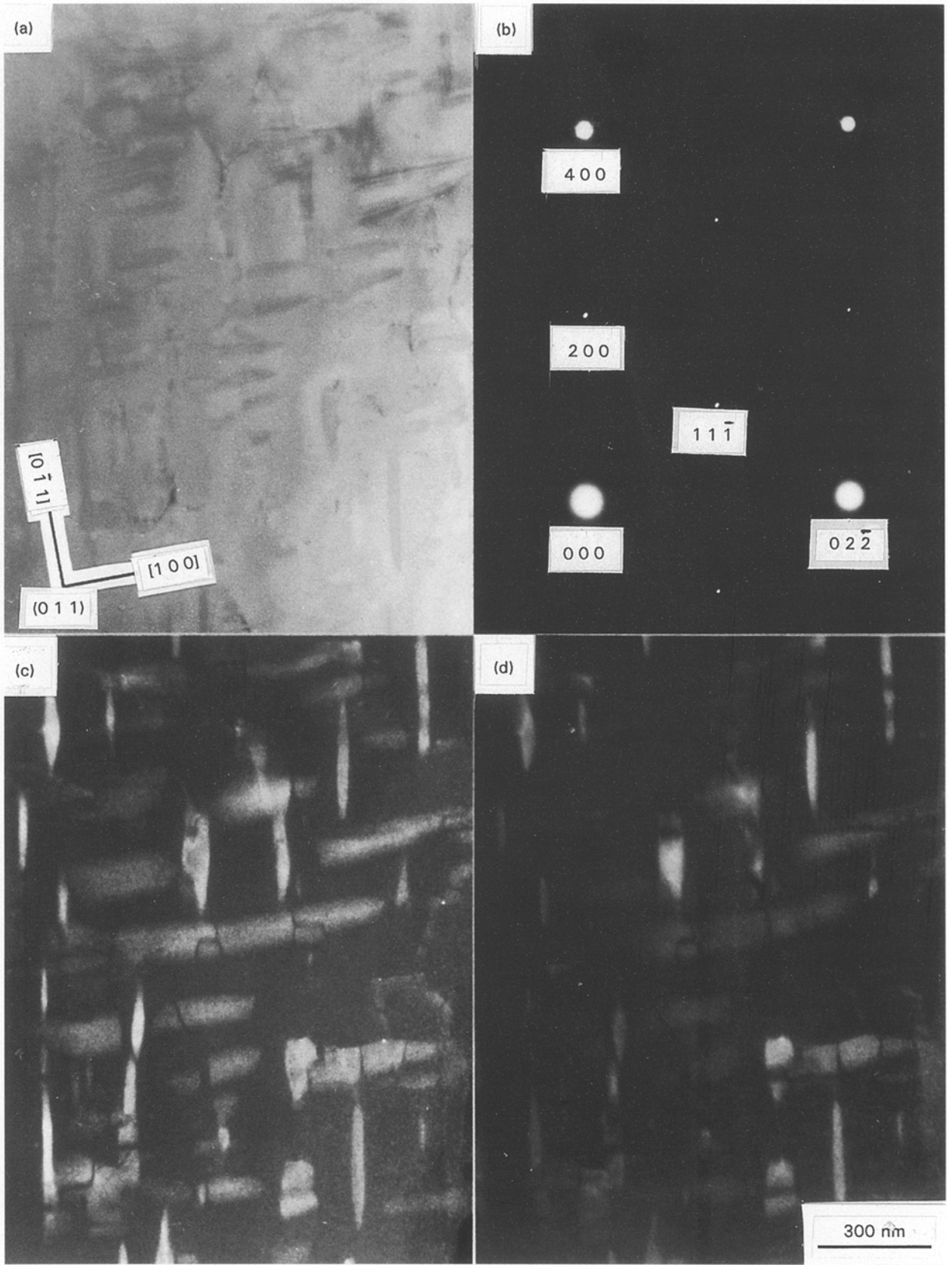

Figure 4 (a) Bright-field image, (b) diffraction pattern, (c) 2 0 0 and (d) 1 1 $\bar{1}$ dark-field images of Fe–5.7 at % Si–6.1 at % Ge alloy (H) annealed at 823 K for 2.6 Ms, showing the two-phase microstructure consisting of A2 and $D0_3$ phases.

4.2. Effect of ferro-magnetism on phase equilibria

By comparison of Fig. 8 with Fig. 10d, the equi-Curie temperature line is found to cross the two-phase field at 973 K. The phase equilibria in this system seem to be influenced by the magnetic transformation. To clarify the influence, we calculated the equilibria with and without the magnetic interactions, and estimated the

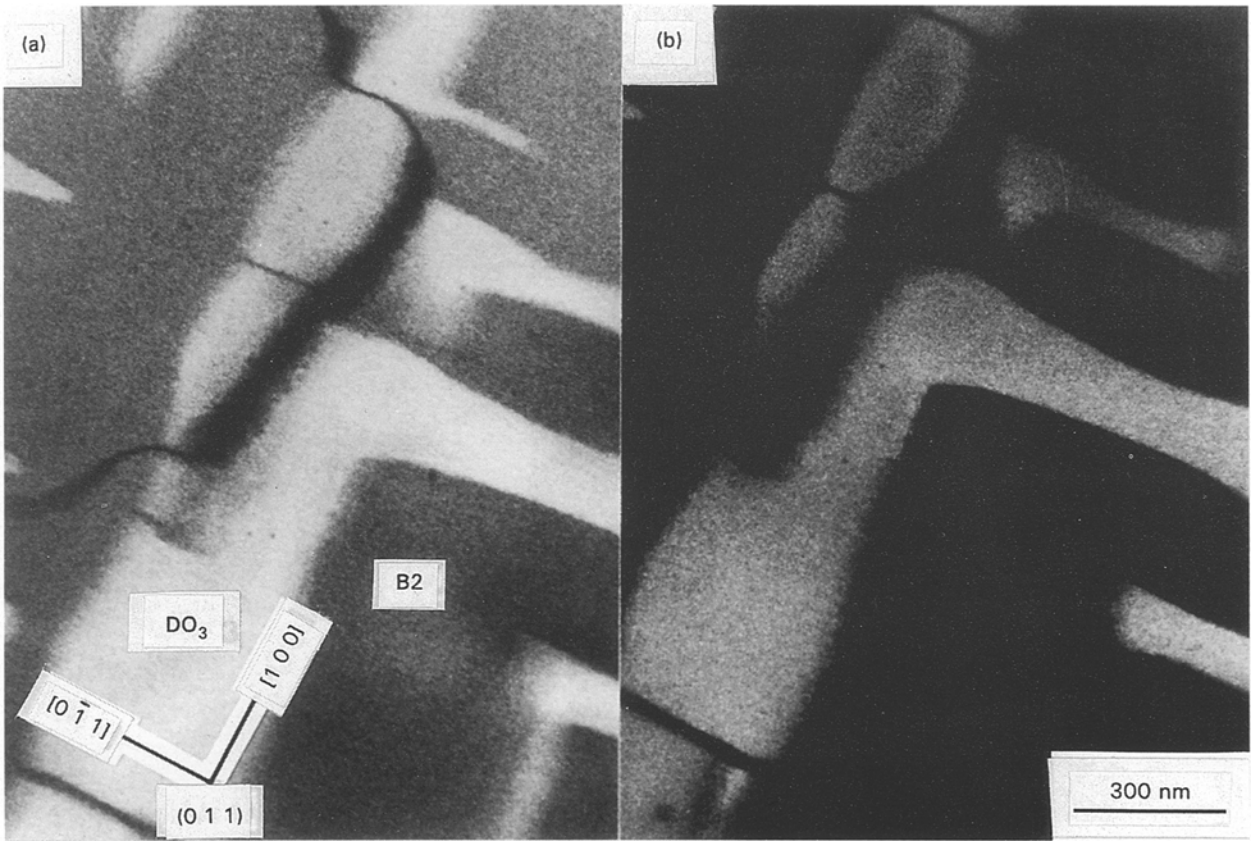

Figure 5 Dark-field images taken from (a) 2 0 0 and (b) 1 1 $\bar{1}$ spots of Fe–7.3 at % Si–6.9 at % Ge alloy (L) annealed at 973 K for 170 ks, showing (B2 + $D0_3$) two-phase microstructure.

effect of the ferro-magnetism on the phase equilibria. Fig. 11 shows the phase diagram at 923 K calculated in the para-magnetic state. The ferro-magnetism gives two types of coexistent A2 + $D0_3$ and B2 + $D0_3$ as shown in Fig. 10c, while in the para-magnetic state B2 single-phase region connects the Fe–Si binary side with the Fe–Ge side and the A2 + $D0_3$ region disappears. Fig. 12 shows the free-energy curves along the tie line (a–b) of A2 + $D0_3$ phase separation at 923 K (Fig. 10c). In the para-magnetic state, B2 structure is more stable than A2, so that the phase separation into B2 and $D0_3$ phases is realized. However, in the ferro-magnetic state, because the A2 phase is more stabilized by the magnetic excess free energy, the A2 + $D0_3$ phase separation appears. The influence of the magnetic transformation is clearly represented in a pseudo-binary vertical section diagram (Fig. 13). In the ferro-magnetic diagram the A2 + $D0_3$ two-phase region expands at the lower temperatures than the magnetic transformation line, particularly towards the $D0_3$ single-phase region, while in the para-magnetic state the expansion has never been recognized and the coexistent phases are not A2 + $D0_3$, but B2 + $D0_3$.

5. Conclusions

Phase separation in iron-rich Fe–Si–Ge ordering alloys was investigated by transmission electron microscopy and thereby isothermal section diagrams were proposed at 823, 873, 923 and 973 K. Section diagrams were calculated based upon the Bragg–Williams–Gorsky model and the ferro-magnetic effects on the phase equilibria were discussed. The following results were obtained.

1. An A2 + $D0_3$ two-phase field exists as a band-shaped region in the iron-rich corner, which links to the B2 + $D0_3$ fields of both Fe–Ge and Fe–Si binary systems.
2. With an increase in temperature, the A2 + $D0_3$ field shrinks towards the middle part of the band region and eventually fades out at 973 K.
3. The isothermal section diagrams determined experimentally are well reproduced by the calcalutions based on the B–W–G approximation.
4. The magnetic transformation has two effects on the equilibria: the appearance of an A2 + $D0_3$ two-phase field and the expansion of the two-phase region.

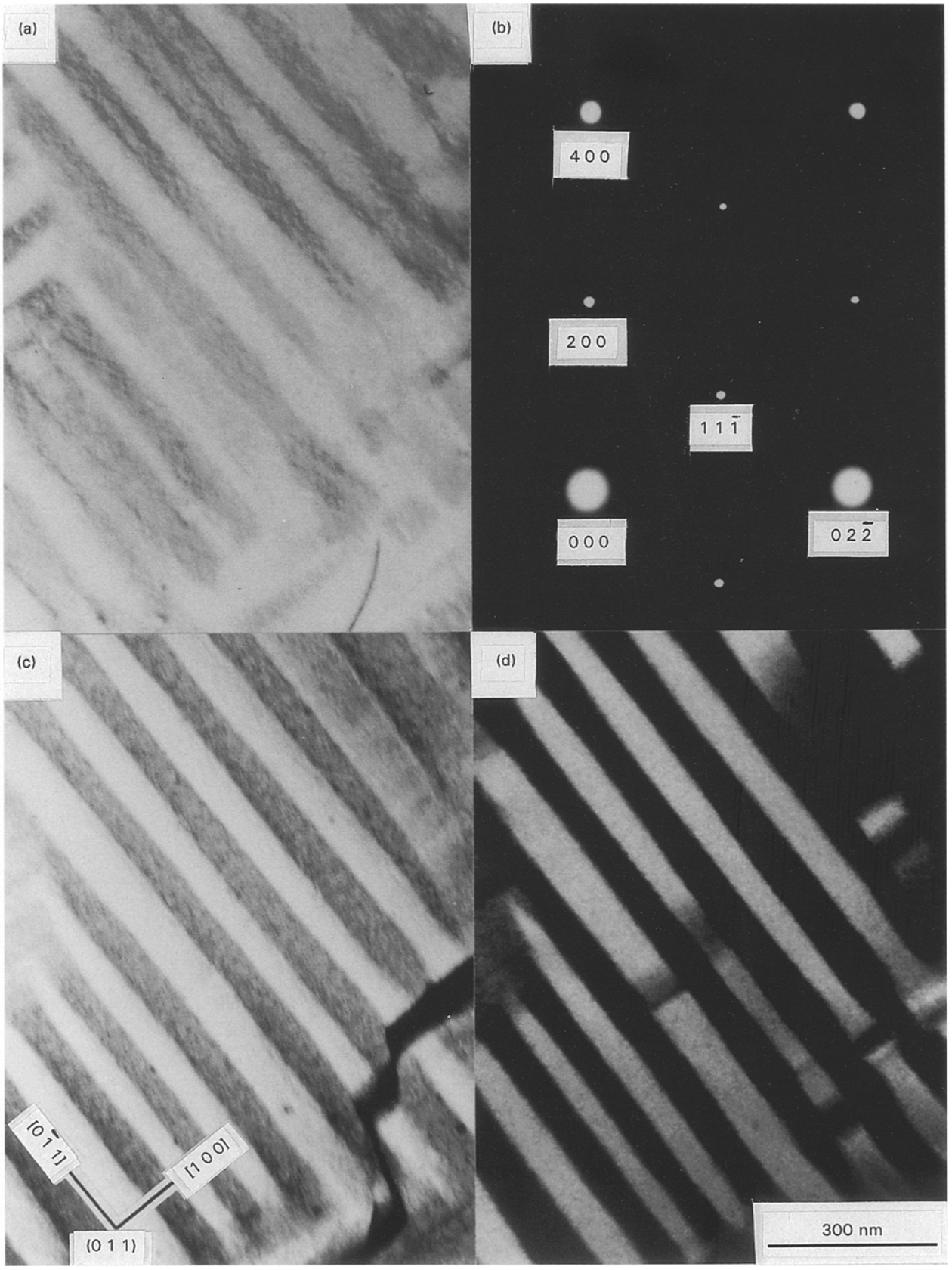

Figure 6 Transmission electron micrographs of Fe–12.6 at % Si–1.2 at % Ge alloy (I) annealed at 923 K for 350 ks. (a) Bright-field image, (b) diffraction pattern, (c) 2 0 0 and (d) 1 1 $\bar{1}$ dark-field images. Rod- or plate-shaped $D0_3$ phases are formed in the B2 matrix.

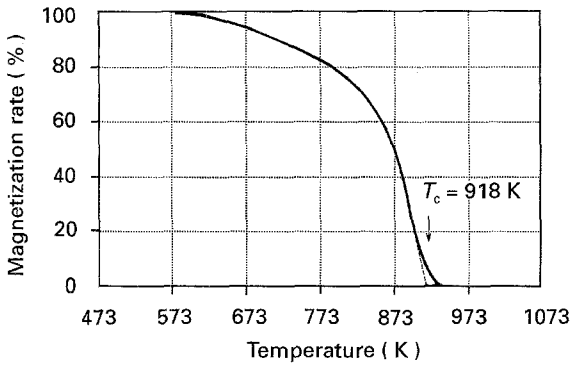

Figure 7 The thermo-magnetization curve of liquid-quenched Fe–9.6 at % Si–7.6 at % Ge alloy (CC). The Curie temperature of this alloy is estimated to be 918 K.

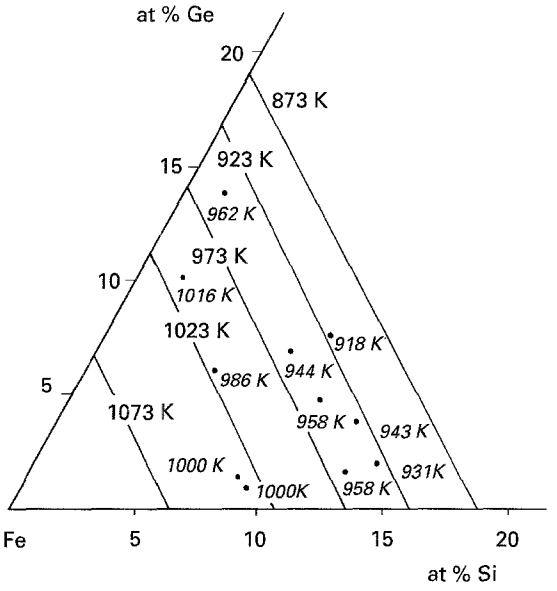

Figure 8 Curie temperatures of liquid-quenched alloys and calculated equi-Curie temperature lines.

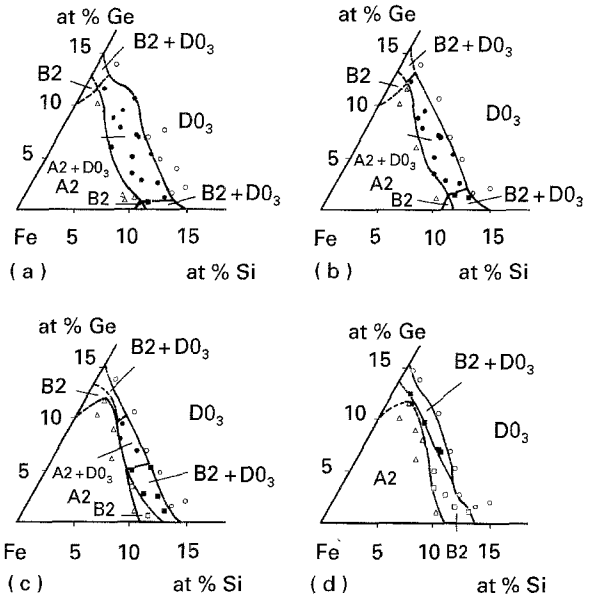

Figure 9 Experimental isothermal section diagrams of the iron-corner of the Fe–Si–Ge ternary system at (a) 823 K, (b) 873 K, (c) 923K and (d) 973K. (△) A2 (○) DO_3, (□) B2, (●) A2 + DO_3, (■) B2 + DO_3.

TABLE II 1st[(1)] and 2nd[(2)] nearest neighbour chemical and magnetic interchange energies used in the calculation. Numerical values are normalized by the Boltzmann constant, $K(=1.38 \times 10^{-23}\text{J})$

	$W^{(1)}$	$W^{(2)}$	$J^{(1)}$	$J^{(2)}$
Fe–Si	$1880k$	$800k$	–	–
Fe–Ge	$2000k$	$920k$	–	–
Si–Ge	$-150k$	$-550k$	–	–
Fe–Fe	–	–	$-196k$	$69k$

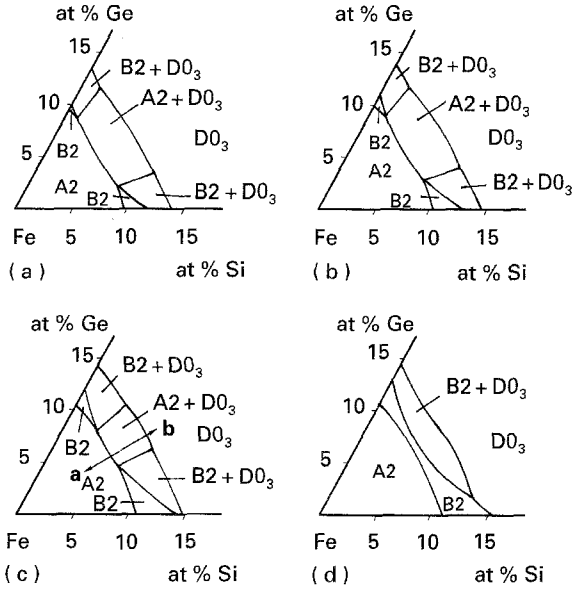

Figure 10 Calculated section diagrams of the Fe–Si–Ge system at (a) 823 K, (b) 873 K, (c) 923 K and (d) 973 K.

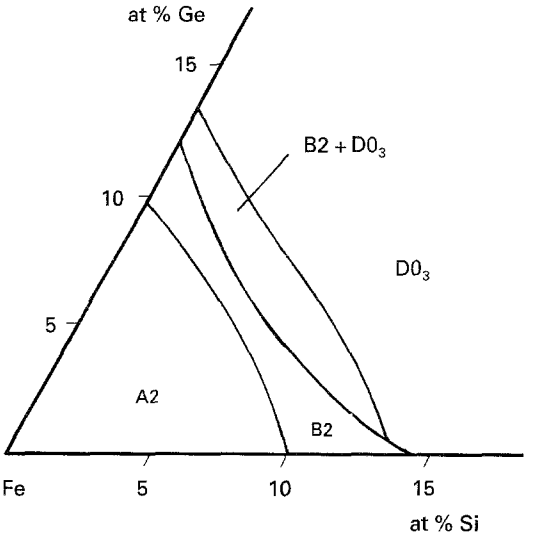

Figure 11 The para-magnetic phase diagram of the Fe–Si–Ge system calculated at 923 K.

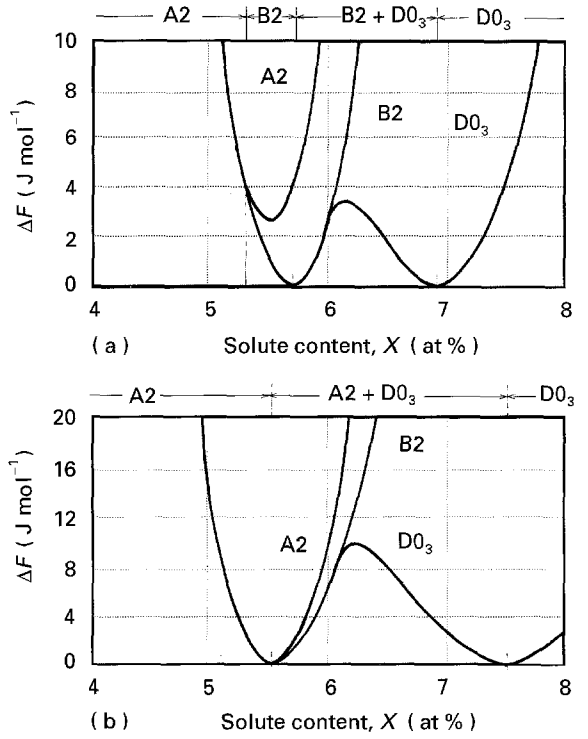

Figure 12 Free-energy curves with composition in (a) para- and (b) ferro- magnetic states for the Fe–X at % Si–X at % Ge system. The energies are normalized by the common tangent line of the phase separation.

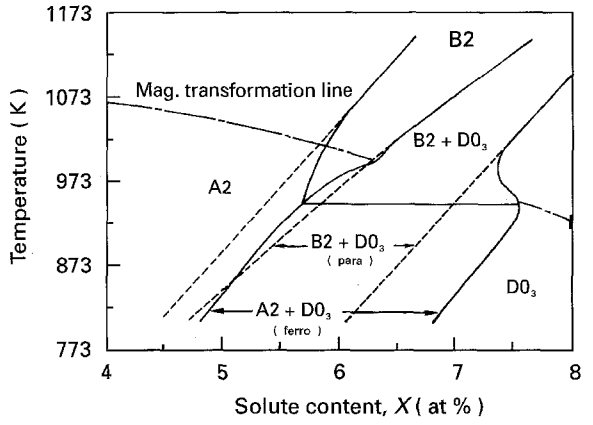

Figure 13 Vertical section diagram along the line connecting pure iron with SiGe. (—) Ferro-magnetic state, (– – –) para-magnetic state. Stabilization and expansion of the A2 + $D0_3$ two-phase field are recognized.

Acknowledgements

We thank Mr S. Hamano for his help with experiments, and Dr M. Doi and Mr T. Koyama for valuable discussions.

References

1. G. SCHLATTE and G. INDEN, *Z. Metallkde* **66** (1975) 660.
2. H. WARLIMONT, *ibid.* **59** (1968) 595.
3. G. INDEN and W. PITSCH, *ibid.* **63** (1972) 253.
4. *Idem, ibid.* **62** (1971) 627.
5. H. ENOKI, K. ISHIDA and T. NISHIZAWA, *Metal. Trans.* **18A** (1987) 949.
6. P.Z. ZHAO, T. KOZAKAI and T. MIYAZAKI, *J. Jpn Inst. Met.* **54** (1990) 1056 (in Japanese).
7. T. KOZAKAI and T. MIYAZAKI, in "Proceedings of 1st Japanese International SAMPE Symposium on New Materials and Processes for the Future", (Yokohama 1989) p.139.
8. T. KOZAKAI and T. MIYAZAKI, in "Computer Aided Innovation of New Materials II", edited by M. Doyama *et al.*, (North-Holland, Amsterdam, 1993) p.767.
9. M. FUKAYA, T. KOZAKAI and T. MIYAZAKI, *J. Jpn Inst. Met.* **52** (1988) 369 (in Japanese) :
10. P.Z. ZHAO, T. KOZAKAI and T. MIYAZAKI, *ibid.* **54** (1990) 139 (in Japanese).
11. T. MIYAZAKI, T. KOZAKAI and T. TSUZUKI, *J. Mater. Sci.* **21** (1986) 2557.
12. M. FUKAYA, T. MIYAZAKI, P.Z. ZHAO and T. KOZAKAI, *ibid.* **25** (1990) 522.
13. T. KOZAKAI and T. MIYAZAKI, *ISI J. Int.* **34** (1994) 373.

Received 22 December 1994
and accepted 2 May 1995